The Canadian Mineralogist
Vol. 44, pp. 1099-1107 (2006)

THE PYROPHANITE–GEIKIELITE SOLID-SOLUTION SERIES: CRYSTAL STRUCTURES OF THE $Mn_{1-x}Mg_xTiO_3$ SERIES ($0 < x < 0.7$)

RUSLAN P. LIFEROVICH AND ROGER H. MITCHELL[¶]

Department of Geology, Lakehead University, 955 Oliver Road, Thunder Bay, Ontario P7B 5E1, Canada

ABSTRACT

Members of the pyrophanite–geikielite solid-solution series, $Mn_{1-x}Mg_xTiO_3$ ($0 < x < 0.7$ *apfu* Mg), were obtained by solid-state synthesis at 1000°C at ambient pressure in air. In common with ilmenite, ternary Mn–Mg titanates adopt ordered $R\bar{3}$ structures. The maximum solubility of Mg in $MnTiO_3$ under the given conditions is considered to be ~0.6 *apfu* Mg, as compounds with greater Mg content could not be synthesized. The structures of these titanates were refined by the Rietveld method from powder X-ray-diffraction data. Within the solid-solution series, unit-cell parameters and unit-cell volumes decrease with increase in Mg content. All compounds consist of distorted TiO_6 and AO_6 (A = Mn,Mg) octahedra, and in common with geikielite, pyrophanite, and ilmenite (*sensu lato*), the TiO_6 octahedra are distorted to a greater degree than $(Mn,Mg)O_6$. The extent of displacement of (Mn,Mg) and Ti from the centers of their coordination polyhedra varies irregularly with increasing Mg content, reaching a maximum for $x = 0.1$ and 0.2 *apfu* Mg. Entry of Mg^{2+} into the ^{VI}A site results in "puckering" of layers consisting of TiO_6 octahedra (less distorted) above and below planes parallel to (001), and decreased "puckering" of the AO_6 octahedra (more distorted). The interlayer distance across the vacant octahedral site in the TiO_6 layer decreases regularly with entry of the smaller Mg^{2+} cation into the ^{VI}A site. The absence of natural solid-solutions between geikielite and pyrophanite seems to be due to the contrasting geochemistry of Mn and Mg rather than to crystallochemical reasons.

Keywords: pyrophanite, geikielite, titanate, order, ilmenite group, solid solution, distorted octahedra, crystal structure, Rietveld refinement.

SOMMAIRE

Nous avons synthétisé les membres de la solution solide entre pyrophanite et geikielite, $Mn_{1-x}Mg_xTiO_3$ ($0 < x < 0.7$ *apfu* Mg), à l'état solide à 1000°C et pression ambiante dans l'air. Tout comme avec l'ilménite, les titanates ternaires de Mn–Mg adoptent une structure ordonnée $R\bar{3}$. Un maximum d'environ 0.6 *apfu* Mg peut être accommodé dans le $MnTiO_3$ aux conditions employées; nous n'avons pas réussi à synthétiser les composés analogues contenant plus de Mg. Nous nous sommes servis d'un affinement de Rietveld des données obtenues par diffraction X sur poudre pour établir la structure de ces titanates. Dans cette série, les paramètres réticulaires et le volume de la maille diminuent à mesure qu'augmente la teneur en Mg. Ces compositions contiennent toutes des octaèdres TiO_6 et AO_6 (A = Mn,Mg) difformes, et tout comme dans la geikielite, la pyrophanite, et l'ilménite (*sensu lato*), les octaèdres TiO_6 sont plus difformes que les octaèdres $(Mn,Mg)O_6$. Le déplacement de (Mn,Mg) et Ti du centre de leurs polyèdres de coordinence varie de façon irrégulière avec l'augmentation en Mg, et atteint son maximum pour $x = 0.1$ et 0.2 *apfu* Mg. L'incorporation du Mg^{2+} dans le site ^{VI}A mène à un froncement des couches d'octaèdres TiO_6 (rendus moins difformes) par dessus et par dessous les plans parallèles à (001) et à une diminution du froncement des octaèdres AO_6 (rendus plus difformes). La distance intercouche près de la lacune octaédrique dans la couche d'octaèdres TiO_6 diminue régulièrement à mesure que le Mg, de plus petit rayon, augmente dans le site ^{VI}A. L'absence d'exemples naturels de la solution solide entre geikielite et pyrophanite semble attribuable aux différences dans le comportement géochimique de Mn et Mg plutôt qu'à une raison cristallochimique.

(Traduit par la Rédaction)

Mots-clés: pyrophanite, geikielite, titanate, ordre, groupe de l'ilménite, solution solide, octaèdres difformes, structure cristalline, affinement de Rietveld.

[¶] *E-mail address*: rmitchel@lakeheadu.ca

Introduction

Ordered rhombohedral titanates, $A^{2+}TiO_3$ (where $^{VI}A^{2+}$ represents a first-row transition metal), are isostructural with ilmenite *sensu lato*. The natural titanates are ilmenite, pyrophanite, geikielite, and ecandrewsite (A = Fe, Mn, Mg, and Zn, respectively). These minerals are common accessories in primary and secondary parageneses in many igneous and metamorphic rocks. Geikielite is an important accessory in kimberlites, lamproites, mantle-derived ultramafic xenoliths, and is also known in skarns developed at the expense of dolostones. Pyrophanite is typical of metamorphosed manganiferous rocks and evolved siliceous and peralkaline silica-undersaturated rocks and their postmagmatic derivatives (Deer *et al*. 1992, Khomyakov 1995, Pekov 2001, Mitchell & Liferovich 2004a). The majority of natural titanates are represented by ferrous solid solutions involving the ilmenite component, and data for iron-poor to iron-free varieties are scarce.

In terms of isovalent diadochy at the $^{VI}A^{2+}$ site, the ilmenite–ecandrewsite ($Fe^{2+}_{1-x}Zn_xTiO_3$), ilmenite – pyrophanite – geikielite ($Fe_{1-[x+y]}Mn_xMg_yTiO_3$), and pyrophanite – ecandrewsite ± ilmenite ($Mn_{1-[x+y]}Zn_xFe_yTiO_3$, $x >> y$) continuous ordered solid-solutions are known to exist in nature (Plimer 1990, Whitney *et al*. 1993, Mitchell & Liferovich 2004a). Of these, the $Mg_{1-x}Zn_xTiO_3$ series and $Mn_{1-x}Zn_xTiO_3$ series have been recently synthesized, and their crystal structures characterized in detail (Liferovich & Mitchell 2004, Mitchell & Liferovich 2004b). Here, we focus on the solid-solution series between pyrophanite and geikielite. The main objective of this study is to determine the limit of solid solution between Mn and Mg in ilmenite-structured titanates at 1000°C at ambient pressure in air. In this contribution, we also describe the response of the ordered $R\bar{3}$ structure to the replacement of Mn^{2+} by the smaller Mg^{2+} cation. This is the first systematic study of the $Mn_{1-x}Mg_xTiO_3$ solid solution adopting the $R\bar{3}$ ilmenite structure.

Background Information

Given the existence of natural manganoan ferroan geikielite and magnesian ferroan pyrophanite, described from carbonatites and jacupirangites occurring at the Jacupiranga complex, Brazil (Gaspar & Wyllie 1983), a perfect solid-solution between pyrophanite and geikielite can be assumed. Magnesium and manganese have the greatest difference in ionic radius (Shannon 1976) of the cations that might adopt the ilmenite structure in combination with Ti in natural systems, *i.e.* $^{VI}R_{Mg}{}^{2+} \approx {}^{VI}R_{Zn}{}^{2+} < {}^{VI}R_{Fe}{}^{2+} < {}^{VI}R_{Mn}{}^{2+}$ (0.72, 0.74, 0.78, and 0.83 Å, respectively). This difference in radii might hinder crystallization of pyrophanite–geikielite solid-solutions in nature, although our reconnaissance study has demonstrated the stability of intermediate compounds in the $Mn_{1-x}Mg_xTiO_3$ and $Mn_{1-2x}Zn_xMg_xTiO_3$ series (Liferovich & Mitchell 2005, 2006).

The $Mn_{1-x}Mg_xTiO_3$ series has not been previously synthesized. The series is of interest to both geoscientists and solid-state chemists because of the expected strong distortion of AO_6 coordination polyhedra due to replacement of $^{VI}Mn^{2+}$ by the relatively smaller $^{VI}Mg^{2+}$. By analogy with the extensive solid-solutions found for the $Fe_{1-x}Mg_xTiO_3$ [$0 \le x \le 0.7$ *apfu* Mg (atoms per formula unit)], $Fe_{1-x}Mn_xTiO_3$ ($0 \le x \le 0.64$ *apfu* Mn), $Mn_{1-x}Zn_xTiO_3$ and $Mg_{1-x}Zn_xTiO_3$ ($0 \le x \le 0.8$ *apfu* Zn) (Deer *et al*. 1992, Mitchell & Liferovich 2004b, Liferovich & Mitchell 2004, respectively), we expected to find an extensive solid-solution between $MnTiO_3$ and $MgTiO_3$.

In this paper, we describe the preparation and structure determination of the $Mn_{1-x}Mg_xTiO_3$ solid-solution series over a range of the Goldschmidt tolerance factor (t), which is a measure of the size mismatch between the A and B cations and an anion for ternary compounds (Goldschmidt 1926). These values range from 0.786 to 0.763 (Table 1) and are relatively high for ilmenite-structured titanates, for which t is usually less than 0.75 (Mitchell 2002).

The Structure of Ilmenite

The ilmenite structure has a $R\bar{3}$ rhombohedral cell. It is an ordered derivative of the archetype corundum structure (space group $R\bar{3}c$) and has been considered in detail by Mitchell & Liferovich (2004b, Fig. 1 therein). Briefly, the ilmenite-type structure is adopted by an $ATiO_3$ titanate as a result of the ordered distribution of A^{2+} and Ti^{4+} cations in two-thirds of the octahedral interstices available in *hcp* oxygen layers in cases where $^{VI}R_A{}^{2+} \approx {}^{VI}R_{Ti}{}^{4+}$, $^{VI}R_A << R_O{}^{2-}$, and the Goldschmidt tolerance factor is close to 0.75 (Mitchell 2002). Thus the ilmenite structure contains equal amounts of di- and tetravalent cations, ordered along the layers and alternating along the c dimension of the unit cell. All the cations are located on the threefold axes, and the only variable positional parameter is z_i. Deviation of z_A and z_{Ti} from their theoretical values, $^1/_3$ and $^1/_6$, respectively, are indicative of "puckering" of cation layers above and below planes parallel to (001) (Wechsler & Prewitt 1984). Cations in the ilmenite structure are displaced from the centroids of octahedra, resulting in distortion of the coordination polyhedra. In general, the AO_6 polyhedron is significantly less distorted than the TiO_6 polyhedron (Mitchell 2002).

Rhombohedral ternary titanates are known to undergo compositionally and *PT*-driven polymorphic modifications to structures similar to those of $LiNbO_3$ and $GdFeO_3$ (space groups $R3c$ and $Pbnm$, respectively: Syono *et al*. 1969, Ko & Prewitt 1988). These transformations are complex, and their study is hindered by kinetic factors and hysteresis effects (Mitchell 2002). Discussion of possible complex interactions, such as

TABLE 1. SELECTED REFINEMENT-PARAMETERS AND CRYSTALLOGRAPHIC CHARACTERISTICS OF SYNTHETIC $Mn_{1-x}Mg_xTiO_3$ SOLID-SOLUTION SERIES AT AMBIENT CONDITIONS

		$MnTiO_3$	$x = 0.1$	$x = 0.2$	$x = 0.3$	$x = 0.4$	$x = 0.5$	$x = 0.6$	$MgTiO_3$
$^{VI}R_A^{2+}$	Å	0.83	0.82	0.81	0.80	0.79	0.78	0.76	0.72
t *		0.786	0.783	0.779	0.775	0.771	0.767	0.763	0.748
Refinement parameters									
$ATiO_3$	%	-	97.79	97.25	96.88	91.76	93.62	~90	~95
Other phases	%	-	Rt 2.21	Rt 2.75	Rt 3.12	Rt 3.03 Arm 5.21	Rt 1.46 Per 0.88 Arm 5.51	Arm≥5	Arm≥5
R_{wp}		-	14.30	13.24	13.16	13.28	13.39	14.16	13.37
R_{Bragg}		-	2.96	2.86	2.30	3.02	2.68	2.95	4.57
GOF		-	1.39	1.35	1.36	1.40	1.36	1.45	1.60
DW		-	1.28	1.27	1.26	1.18	1.29	1.09	0.95
Unit-cell characteristics									
a	Å	5.139(0)	5.1303(0)	5.1234(0)	5.1149(0)	5.1084(1)	5.1007(0)	5.0921(0)	5.0567(0)
c	Å	14.283(0)	14.2428(2)	14.2054(2)	14.1614(1)	14.1286(2)	14.0910(1)	14.0532(1)	13.9034(2)
c/a		2.779	2.776	2.773	2.769	2.766	2.763	2.760	2.750
V	Å^3	326.7	324.648(6)	322.923(6)	320.856(6)	319.295(6)	317.490(4)	315.570(5)	307.883(6)
AO_6 octahedron									
<A-O1>	Å	2.195(1)	2.199(10)	2.193(10)	2.180(10)	2.170(7)	2.162(7)	2.151(9)	2.088(7)
V_{AO6}	Å^3	13.350	13.41	13.36	13.16	12.98	12.80	12.64	11.64
A-shift	Å	0.146	0.376	0.373	0.150	0.140	0.132	0.131	0.158
Δ_{AO6}		1.500	1.693	1.760	1.629	1.411	1.253	1.265	1.838
δ_{AO6}		101.58	97.96	95.43	91.18	89.13	92.14	88.39	75.62
TiO_6 octahedron									
<Ti-O1>	Å	1.980(1)	1.969(10)	1.969(10)	1.970(10)	1.973(10)	1.973(7)	1.974(9)	2.005(7)
V_{TiO6}	Å^3	9.97	9.80	9.81	9.82	9.86	9.85	9.86	10.39
Ti-shift	Å	0.186	0.191	0.201	0.189	0.196	0.190	0.186	0.206
Δ_{TiO6}		2.731	2.844	3.178	2.787	2.996	2.861	2.750	3.405
δ_{TiO6}		69.69	70.74	68.91	68.99	68.94	70.31	71.80	61.74

The data of Kidoh *et al.* (1984) were used for $MnTiO_3$. $^{VI}R_A^{2+}$: average radius of cations in A site.
Mineral symbols: Rt: rutile, Per: periclase, Arm: armalcolite.
* Tolerance factor for ABO_3 compounds, $t = (R_O + R_A) / [\sqrt{2}\,(R_O + R_B)]$ (Goldschmidt 1926).
d_i: The distance to the central atom. Δ_n Polyhedron bond-length distortion (see text for details).
δ_n Bond-angle variance (see text for details). - No data available.

first-order and second-order Jahn–Teller effects and "direct $^{VI}A^{2+}$–$^{VI}A^{2+}$ interactions" (Goodenough 1960, Kunz & Brown 1995) are beyond the scope of this reconnaissance study.

Analytical Methods

The synthesis was done in air from stoichiometric amounts of high-purity oxides by routine solid-state ceramic techniques. Analytical methods and the crystal-structure refinement approach, together with the methods for calculation of the crystallochemical parameters of rhombohedral $R\bar{3}$ structures, are described by Mitchell & Liferovich (2004b) and Liferovich & Mitchell (2005). Differences with respect to this work pertain to the temperature of synthesis of the $MgTiO_3$ end-member, which could only be synthesized at 1200°C. We had to use a lower temperature and 12-hours duration of synthesis experiments for the Mn–Mg titanates instead of the much longer times we typically used for other titanates (*i.e.*, 48 hr. sintering after 24 hr. calcination) to avoid oxidation of Mn^{2+}.

Results

Synthetic manganese–magnesium titanates

Our study demonstrated that synthesis of the $Mn_{1-x}Mg_xTiO_3$ ($0 < x < 0.7$) solid-solution series with $x = 0.1$ *apfu* Mg increments is possible at 1000°C at ambient pressure in air. However, pyrophanite ($MnTiO_3$), geikielite ($MgTiO_3$) and $Mn_{1-x}Mg_xTiO_3$ compounds with $0.7 \le x \le 0.9$ *apfu* Mg could not be prepared at this temperature. The $MgTiO_3$ end member,

which does not form at 1000°C, was obtained at a higher temperature (1200°C) and has crystallochemical parameters (see below) similar to those previously published by Wechsler & Von Dreele (1989). Attempts to synthesize Mn-bearing geikielite with 0.7–0.9 *apfu* Mg at temperatures ranging from 1000 to 1200°C failed. We produced instead $Mn_{\sim 0.4}Mg_{\sim 0.6}TiO_3$ titanate plus a manganoan armalcolite-like phase, with the abundance of armalcolite increasing with *x*. Consideration of these "failed" experiments is beyond the scope of the present paper. Quantitative energy-dispersion analyses (EDS) show that all the Mn–Mg titanates obtained at 1000°C approach $ATiO_3$ stoichiometry within the accuracy of determination. The most magnesian titanate obtained in our study ($x = 0.6$ *apfu* Mg) has the composition (wt.%): 17.9(0.1) MgO, 21.6(0.6) MnO, and 60.8(0.3) TiO_2, for a total of 100.3%.

The powder X-ray-diffraction patterns of all titanates synthesized here contain reflections with *h*0*l* (*l* odd) resulting from the ordered distribution of A^{2+} and Ti^{4+} in alternating layers of octahedra (Raymond & Wenk 1971). These reflections are forbidden for the fully disordered corundum-type structure and $LiNbO_3$-type structure, and are not characteristic of either armalcolite or rutile, which occur as minor impurities (≤5 vol. %).

Some Bragg reflections of the armalcolite-like phase [orthorhombic $A^{2+}Ti_2O_5$] are very close to or overlap with the major reflections of the rhombohedral titanate. Overlaps involve the (230), (240), (250), and (630) reflections of armalcolite, and (104), (113), (024), and (030) reflections of $ATiO_3$, respectively. Unfortunately, these overlaps influence the accuracy of the crystal-structure parameters determined by the Rietveld method for the magnesium-rich titanates, and lead to overestimation of the abundance of armalcolite in armalcolite-bearing compounds ($x = 0.5$ and 0.6 *apfu* Mg) as compared to modal analysis using back-scattered electron (BSE) imagery. Nevertheless, the crystal-structure parameters obtained for geikielite ($MgTiO_3$) associated with armalcolite ($MgTi_2O_5$) *sensu stricto* as a minor phase are close to those previously published by Wechsler & von Dreele (1989).

Rietveld Refinement and Geometry of the Cation Sites

For Rietveld refinement, we used the atom coordinates given by Kidoh *et al*. (1984) for synthetic $MnTiO_3$ as a starting model. Figure 1 is a Rietveld refinement plot for synthetic $Mn_{0.7}Mg_{0.3}TiO_3$ titanate. The occupancy of the ^{VI}A site was set in accordance with the target solid-solution composition during the initial steps, and refined at the final steps of the procedure, with the total occupancy of the *Ti* and *A* sites constrained to be unity. At a final step of the refinement procedure, we attempted to refine occupancies of the ^{VI}A and ^{VI}Ti sites to test the possible entry of the divalent cation(s) or Mn^{3+} and Mn^{4+} cations, if any, into the ^{VI}Ti position and *vice versa*. These refinements converged easily (in

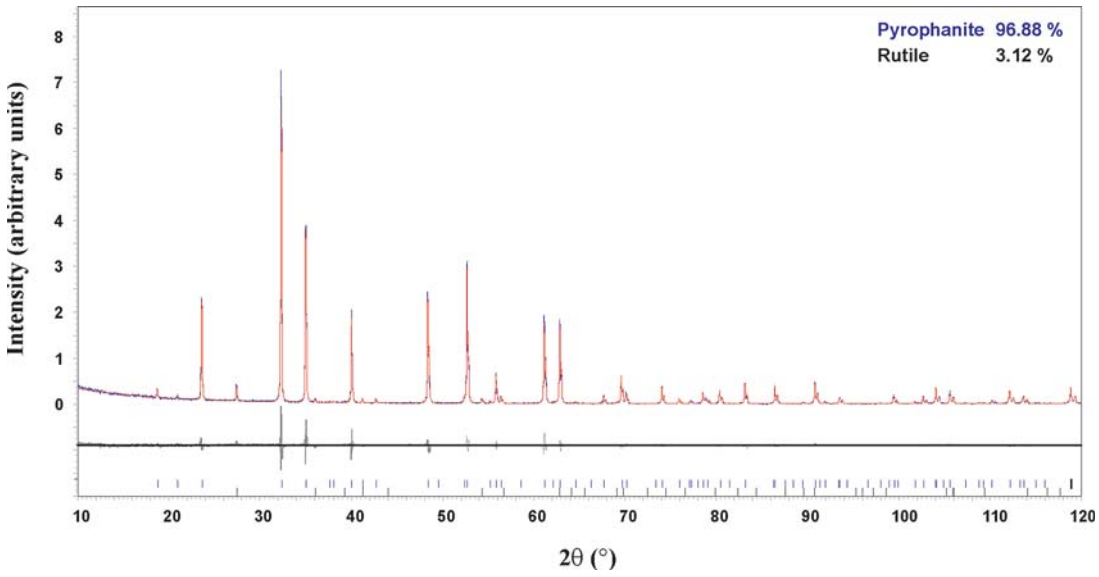

FIG. 1. Rietveld refinement plot (line) of the powder X-ray-diffraction data for $Mn_{0.7}Mg_{0.3}TiO_3$ at room temperature (dots). Lower bars pertain to the peaks of rutile. The difference curves between observed and calculated profiles are plotted. For agreement factors, see Table 1.

a few steps) and did not induce statistically significant changes in any of the refined parameters. The refined occupancies of both octahedral sites do not deviate from the target stoichiometry within the range of one estimated standard deviations (e.s.d.), *i.e.,* neither the presence of Ti in the ^{VI}A site or any of the divalent cations or oxidized Mn in the ^{VI}Ti site is indicated within the accuracy of the Rietveld method. Lack of detectable Mn-for-Ti substitution in the $ATiO_3$ compounds implies the absence of significant oxidation of Mn to the smaller Mn^{3+} (^{VI}R = 0.65 Å) and Mn^{4+} (^{VI}R = 0.53 Å) cations. These, if present, have to share a site with similar-sized Ti^{4+} (^{VI}R = 0.605 Å) rather than with the significantly larger Mn^{2+} (^{VI}R = 0.83 Å) and Mg^{2+} (^{VI}R = 0.72 Å; radii from Shannon 1976). Thus we are confident that manganese is not oxidized to higher valences in the titanates synthesized and considered in this work.

The above implies that detectable disorder is absent from compounds considered here, which agrees with the presence in their XRD patterns of the sharp *h*0*l* (*l* odd) reflections (Fig. 2), which are known to result from A^{2+}–Ti^{4+} ordering (Raymond & Wenk 1971). These should become diffuse-to-absent in the case of disorder of the octahedrally coordinated cations.

The refinement and unit-cell parameters, polyhedron volumes, shifts (displacements) of $^{VI}A^{2+}$ and $^{VI}Ti^{4+}$ atoms from the centers of coordination polyhedra, and parameters describing the distortion of coordination polyhedra (see below) in the titanates synthesized are summarized in Table 1. As expected, entry of the smaller Mg^{2+} cation at the AO_6 site results in a regular decrease in the unit-cell parameters and unit-cell volume with increasing Mg content (Fig. 2).

Atom coordinates and isotropic displacement factors are summarized in Table 2. Selected bond-lengths and bond-angles within and outside of the first coordination spheres of the *A* and Ti cations are listed in Appendix 1.

We employ the Δ_6 distortion index introduced by Shannon (1976) to illustrate polyhedron distortion, given as $\Delta_n = 1/n \bullet \Sigma\{(r_i - \bar{r}) / \bar{r}\}^2 \bullet 10^3$, where r_i and $\bar{r}$ are individual and average bond-lengths in the polyhedron, respectively. To characterize deviations from the ideal bond-angles in regular octahedra, we calculate the bond-angle-variance index $\{\delta_n = \Sigma[(\theta_i - 90)^2/(n - 1)]$, where θ_i are the bond angles at the central atom (Robinson *et al*. 1971)$\}$. The indices calculated and the average bond-lengths are given in Table 1.

As might be expected, the <*A*–O> distance decreases with increasing content of $^{VI}Mg^{2+}$, whereas the <Ti–O> distance increases (Table 1, Figs. 3a, b). The resulting *c*/*a* value decreases smoothly with *x* (Table 1, Fig. 2). These changes result in a decrease in the unit-cell volume and unit-cell dimensions through the series, in good agreement with the entry of the smaller Mg^{2+} cation into the layers of AO_6 octahedra. Polyhedron volumes change antipathetically (Table 1, Figs. 3a, b). The *z* coordinate of the *A* cations approaches the theoretical value of one-third with increasing Mg-for-Mn substitution. On the contrary, the *z* coordinate of the Ti cations deviates from the theoretical value of one-sixth with increasing *x* (Fig. 2). The change in *z*

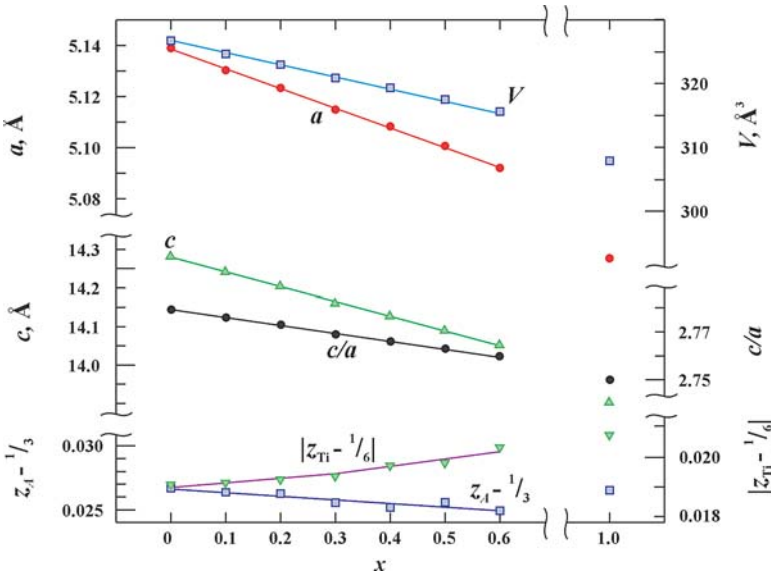

FIG. 2. $Mn_{1-x}Mg_xTiO_3$ series: variation of the unit-cell parameters and volumes with composition. Note: error bars are less than the size of the dots employed for plotting (Table 1).

coordinate is in agreement with displacement of the *A* cations from the center of the AO_6 coordination polyhedra (Table 1). The displacement of the Ti cations also increases regularly (Table 1), as illustrated by the parameter $|z_{Ti} - {}^1/_6|$, which describes the displacement of $^{VI}Ti^{4+}$ from the ideal position, and which increases with *x* (Fig. 2). Because of the greater displacement of the A^{2+} cations, the layer consisting of AO_6 octahedra is more "puckered" above and below planes parallel to (001) (Wechsler & Prewitt 1984) than the layer composed of TiO_6 octahedra, but becomes less distorted with increasing *x*, whereas there is an increase in the "puckering" of the layer of TiO_6 octahedra above and below planes parallel to (001). The *A*–*A* distance across the vacant octahedral site in the TiO_6 layer decreases with entry of the smaller $^{VI}Mg^{2+}$ cation into the *A* site (Appendix 1).

The synthetic $Mn_{1-x}Mg_xTiO_3$ titanates contain distorted coordination polyhedra similar to those occurring in pyrophanite and ilmenite *sensu lato*. The AO_6 octahedra exhibit less distortion than the TiO_6 octahedra, as illustrated by bond-length-based indices of distortion, Δ_{AO6} and Δ_{TiO6} (Table 1). The overall distortion of the AO_6 octahedra depends on the extent of Mg-for-Mn substitution in the range $0.1 \le x \le 0.5$, and decreases with increasing *x*. For *x* above 0.5 *apfu* Mg, the distortion remains constant. Distortion of the TiO_6 octahedra is less dependent on $^{VI}Mn^{2+} \rightleftharpoons {}^{VI}Mg^{2+}$ diadochy. Indices of bond-angle variance (δ_6) are less sensitive to shrinkage of the AO_6 polyhedra and exhibit an overall decrease with *x* (Fig. 3a). Indices of bond-angle variance in the TiO_6 octahedron do not vary significantly (Fig. 3b).

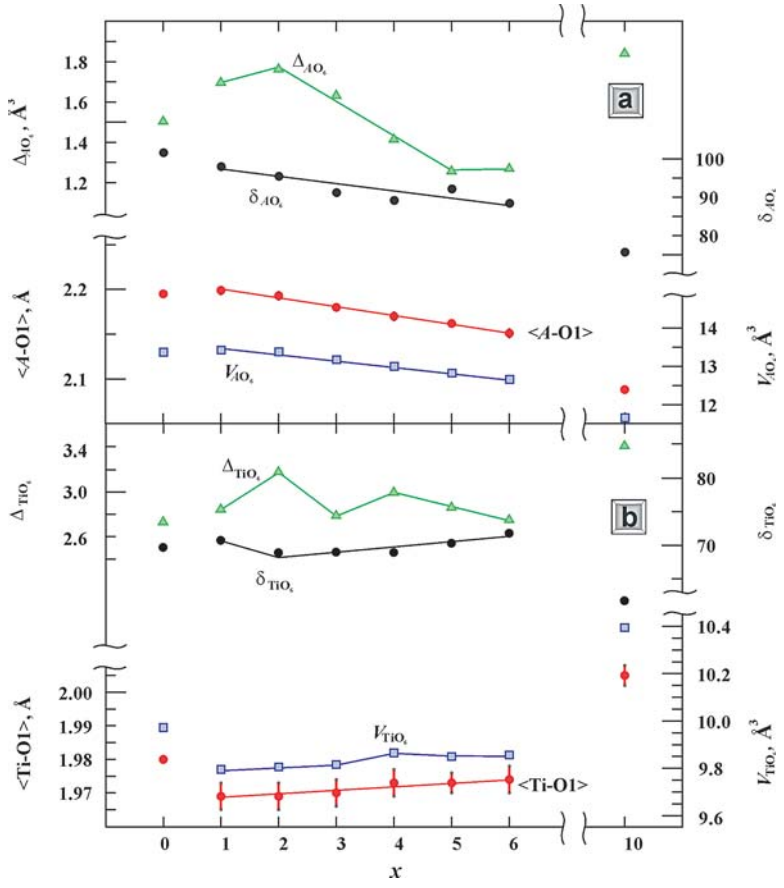

FIG. 3. $Mn_{1-x}Mg_xTiO_3$ series: variation of the volume of coordination polyhedra, their distortion parameters (*see* text), and displacement of the *A* and Ti cations from the centers of the coordination polyhedra with composition. Note: error bars for volumes of polyhedra are less than the size of symbol on the plot (Table 1).

TABLE 2. POSITIONAL PARAMETERS AND ISOTROPIC DISPLACEMENT FACTORS (Å^2) FOR SYNTHETIC $Mn_{1-x}Mg_xTiO_3$ SOLID-SOLUTION SERIES AT AMBIENT CONDITIONS

Position	Sample	*x*	*y*	*z*	B_{iso}
^{VI}A	$MnTiO_3$*	0	0	0.36002(1)	-
	x = 0.1	0	0	0.35970(10)	0.55(4)
	x = 0.2	0	0	0.35960(11)	0.58(4)
	x = 0.3	0	0	0.35888(12)	0.47(4)
	x = 0.4	0	0	0.35852(15)	0.44(5)
	x = 0.5	0	0	0.35891(13)	0.49(3)
	x = 0.6	0	0	0.35827(17)	0.46(4)
	$MgTiO_3$	0	0	0.35986(10)	0.47(4)
^{VI}Ti	$MnTiO_3$*	0	0	0.14758(1)	-
	x = 0.1	0	0	0.14752(11)	0.42(4)
	x = 0.2	0	0	0.14741(11)	0.21(4)
	x = 0.3	0	0	0.14730(12)	0.19(4)
	x = 0.4	0	0	0.14694(14)	0.37(4)
	x = 0.5	0	0	0.14685(11)	0.27(3)
	x = 0.6	0	0	0.14632(14)	0.28(3)
	$MgTiO_3$	0	0	0.14590(10)	0.54(4)
O(1)	$MnTiO_3$*	0.31890(10)	0.03100(10)	0.24393(3)	-
	x = 0.1	0.31989(61)	0.03003(83)	0.24268(34)	0.46(6)
	x = 0.2	0.32138(60)	0.03023(82)	0.24304(29)	0.42(6)
	x = 0.3	0.31926(6)	0.02725(8)	0.24314(25)	0.28(6)
	x = 0.4	0.31943(59)	0.02780(82)	0.24401(24)	0.34(6)
	x = 0.5	0.31817(48)	0.02865(62)	0.24469(20)	0.53(5)
	x = 0.6	0.31649(54)	0.02532(73)	0.24459(22)	0.66(6)
	$MgTiO_3$	0.31915(51)	0.02141(74)	0.24575(22)	0.71(4)

* Single-crystal refinement data (Kidoh *et al.* 1984).

CONCLUSIONS

The experimentally obtained limit of substitution of Mn and Mg in the structures of Fe-free $R\bar{3}$ titanates is ~0.6 *apfu* Mg at 1000°C at ambient pressure in an air atmosphere. The experimentally obtained range of Goldschmidt tolerance factors for Mn–Mg titanates adopting the ordered $R\bar{3}$ structure at these conditions ranges from 0.76 to 0.78 (Table 1). Given that $MgTiO_3$ (t = 0.75) adopts the ilmenite structure at 1200°C, we conclude that the limits of stability of the rhombohedral titanates as predicted by the Goldschmidt tolerance factor vary with respect to intensive parameters such as temperature. The complete $Mn_{1-x}Mg_xTiO_3$ series might be successfully synthesized in an O_2-free atmosphere over the temperature range ~950°C < $T \leq$ 1200°C.

The scarcity of natural iron-poor to iron-free rhombohedral titanates of manganese and magnesium is not due to crystallochemical limitations. The ilmenite-structured Mn–Mg solid solutions form in some exotic mineral-forming environments depleted in Fe, which are associated with silica-undersaturated ultramafic–alkaline rocks found with carbonatite complexes such as Jacupiranga (Gaspar & Wyllie 1983). To the best of our knowledge, of these rocks, the most favorable for crystallization of Fe-poor pyrophanite–geikielite solid-solution series are the magnetite-poor magnesiocarbonatite and some rocks of the calciocarbonatite series.

The deviation of the crystallographic characteristics of the high-temperature $MgTiO_3$ and $MnTiO_3$ end members described by Kidoh *et al.* (1984) from an extrapolation of the trend obtained for the synthetic titanates with $0.1 \leq x \leq 0.6$ *apfu* Mg indicates that the parameters of the $R\bar{3}$ crystal structure are dependent on the kinetics of synthesis.

ACKNOWLEDGEMENTS

This work was supported by the Natural Sciences and Engineering Research Council of Canada and Lakehead University (Canada). We are grateful to Allan MacKenzie for assistance with analytical work, and Anne Hammond for sample preparation. The authors are grateful to J.C. Melgarejo, whose constructive criticism resulted in improvements to the initial version of this work. The authors also thank Dr. Robert F. Martin for editorial care in handling of this contribution.

REFERENCES

DEER, W.A., HOWIE, R.A. & ZUSSMAN, J. (1992): *An Introduction to the Rock-Forming Minerals* (2nd ed.). John Wiley & Sons, New York, N.Y.

GASPAR, J.C. & WYLLIE, P.J. (1983): Ilmenite (high Mg,Mn,Nb) in the carbonatites from the Jacupiranga Complex, Brazil. *Am. Mineral.* **68**, 960-971.

GOLDSCHMIDT, V.M. (1926): Geochemische Verteilungsgesetze der Elementer VII. *Skrifter Norsk Vidensk. Akad. Klasse* **1**. *Matematisk, Naturvidenskaplig Klasse*, *Oslo, Norway*.

GOODENOUGH, J.B. (1960): Direct cation–cation interactions in several oxides. *Phys. Rev.* **117**, 1442-1451.

KHOMYAKOV, A.P. (1995): *Mineralogy of Hyperagpaitic Alkaline Rocks*. Clarendon Press, Oxford, U.K.

KIDOH, K., TANAKA, K., MARUMO, F. & TAKEI, H. (1984): Electron density distribution in ilmenite-type crystals. II. Manganese (II) titanium (IV) trioxide. *Acta Crystallogr.* **B40**, 329-332.

KO, JAIDONG & PREWITT, C.T. (1988): High-pressure phase transformation in $MnTiO_3$ from the ilmenite to the $LiNbO_3$ structure. *Phys. Chem. Minerals* **15**, 355-362.

KUNZ, M. & BROWN, I.D. (1995): Out-of-center distortions around octahedrally coordinated d^0-transition metals. *J. Solid State Chem.* **115**, 395-406.

LIFEROVICH, R.P. & MITCHELL, R.H. (2004): Geikielite–ecandrewsite solid solutions: synthesis and crystal structures of the $Mg_{1-x}Zn_xTiO_3$ ($0 \leq x \leq 0.8$) series. *Acta Crystallogr.* **B60**, 496-501.

LIFEROVICH, R.P. & MITCHELL, R.H. (2005): Rhombohedral ilmenite group nickel titanates with Zn, Mg, and Mn: synthesis and crystal structures. *Phys. Chem. Minerals* **32**, 442-449.

LIFEROVICH, R.P. & MITCHELL, R.H. (2006): Mn, Mg, and Zn ilmenite-group titanates: a reconnaissance Rietveld study. *Crystallography Reports, Structure of Inorganic Compounds* **51**, 383-390.

MITCHELL, R.H. (2002): *Perovskites: Modern and Ancient*. Almaz Press, Thunder Bay, Ontario (www.almazpress.com).

MITCHELL, R.H. & LIFEROVICH, R.P. (2004a): Ecandrewsite – zincian pyrophanite from lujavrite, Pilansberg alkaline complex, South Africa. *Can. Mineral.* **42**, 1169-1178.

MITCHELL, R.H. & LIFEROVICH, R.P. (2004b): Pyrophanite–ecandrewsite solid solutions: crystal structures of the $Mn_{1-x}Zn_xTiO_3$ series ($0.1 \leq x \leq 0.8$). *Can. Mineral.* **42**, 1871-1880.

PEKOV, I.V. (2001): *Lovozero Massif: History of Investigations, Pegmatites, Minerals*. Zemlya Press, Moscow, Russia (in Russ.).

PLIMER, I.R. (1990): The ilmenite–ecandrewsite solid solution series, Broken Hill, Australia. *Neues Jahrb. Mineral., Monatsh.*, 529-536.

RAYMOND, K.N. & WENK, H.R. (1971): Lunar ilmenite (refinement of the crystal structure). *Contrib. Mineral. Petrol.* **30**, 135-140.

ROBINSON, K., GIBBS, G.V. & RIBBE, P.H. (1971): Quadratic elongation: a quantitative measure of distortion in coordination polyhedra. *Science* **172**, 567-570.

SHANNON, R.D. (1976): Revised effective ionic radii and systematic studies of interatomic distances in halides and chalcogenides. *Acta Crystallogr.* **A32**, 751-767.

SYONO, Y., AKIMOTO, S., ISHIKAWA, Y. & ENDOH, Y. (1969): A new high pressure phase of $MnTiO_3$ and its magnetic property. *J. Phys. Chem. Solids* **30**, 1665-1672.

WECHSLER, B.A. & PREWITT, C. (1984): Crystal structure of ilmenite ($FeTiO_3$) at high temperature and high pressure. *Am. Mineral.* **69**, 176-185.

WECHSLER, B.A. & VON DREELE, R.B. (1989): Structure refinements of Mg_2TiO_4, $MgTiO_3$ and $MgTi_2O_5$ by time-of-flight neutron powder diffraction. *Acta Crystallogr.* **B45**, 542-549.

WHITNEY, D.L., HIRSCHMANN, M. & MILLER, M.G. (1993): Zincian ilmenite – ecandrewsite from a pelitic schist, Death Valley, California, and the paragenesis of $(Zn,Fe)TiO_3$ solid solution in metamorphic rocks. *Can. Mineral.* **31**, 425-436.

Received February 28, 2005, revised manuscript accepted August 23, 2006.

APPENDIX 1. SELECTED BOND-LENGTHS (Å) AND BOND-ANGLES (°) OF SYNTHETIC $Mn_{1-x}Mg_xTiO_3$ SOLID-SOLUTION SERIES AT AMBIENT CONDITIONS

			$MnTiO_3$	$x = 0.1$	$x = 0.2$	$x = 0.3$	$x = 0.4$	$x = 0.5$	$x = 0.6$	$MgTiO_3$
AO_6 octahedron										
3 × *A*-O1		Å	2.110	2.109(4)	2.101(4)	2.092(4)	2.088(3)	2.085(3)	2.074(3)	1.998(3)
3 × *A*-O1		Å	2.280	2.290(4)	2.285(4)	2.268(4)	2.251(3)	2.238(3)	2.227(4)	2.177(3)
3 × O-*A*-O		°	72.95	72.85	73.29	73.55	74.06	73.99	74.21	77.02
3 × O-*A*-O		°	91.95	92.08	91.97	91.68	91.37	91.01	90.79	87.98
3 × O-*A*-O		°	88.22	88.79	88.43	88.97	88.51	88.14	88.77	88.46
3 × O-*A*-O		°	103.28	102.54	102.64	102.29	102.56	103.15	102.69	103.34
3 × O-*A*-O		°	158.33	158.88	159.05	159.58	159.67	159.13	159.71	161.04
TiO_6 octahedron										
3 × Ti-O1		Å	1.877	1.864(4)	1.858(4)	1.866(4)	1.865(4)	1.867(3)	1.870(4)	1.888(3)
3 × Ti-O1		Å	2.084	2.074(4)	2.080(4)	2.074(4)	2.081(4)	2.078(3)	2.077(3)	2.122(3)
3 × O-Ti-O		°	162.01	162.18	162.40	162.42	162.25	161.92	161.78	162.91
3 × O-Ti-O		°	81.14	81.92	81.96	81.81	81.30	81.25	81.42	84.24
3 × O-Ti-O		°	80.92	80.35	80.53	80.78	81.10	80.78	80.60	79.42
3 × O-Ti-O		°	94.81	93.87	93.84	93.33	93.75	94.35	93.58	92.74
3 × O-Ti-O		°	101.88	102.52	102.35	102.60	102.36	102.15	102.66	101.64
A-Ti		Å	3.034	3.022	3.014	2.996	2.989	2.988	2.978	2.946
A-*A*	*a*	Å	3.063	3.056	3.051	3.040	3.034	3.032	3.022	2.994
A-*A*	*b*	Å	3.999	3.996	3.989	3.997	3.998	3.976	3.984	3.968
Ti-Ti	*a*	Å	3.017	3.012	3.008	3.004	3.001	2.997	2.995	2.978
Ti-Ti	*b*	Å	4.216	4.202	4.188	4.172	4.152	4.138	4.112	4.044
O-O	*c*	Å	2.711	2.719	2.728	2.716	2.712	2.693	2.687	2.711
O-O	*d*	Å	3.309	3.290	3.280	3.259	2.258	3.267	3.240	3.135
O-O	*e*	Å	3.150	3.169	3.157	3.131	3.107	3.085	3.064	2.916
O-O	*f*	Å	3.058	3.080	3.062	3.058	3.031	3.009	3.011	2.903
O-O	*g*	Å	2.914	2.908	2.895	2.912	2.906	2.905	2.920	2.927
O-O	*h*	Å	2.575	2.546	2.551	2.557	2.570	2.574	2.579	2.695
O-O	*i*	Å	2.919	2.880	2.880	2.869	2.884	2.897	2.880	2.907
Ti-O-*A*	*j*	°	118.76	119.16	119.50	119.42	119.38	118.88	118.91	120.37
A-O-*A*	*k*	°	88.41	87.91	88.03	88.32	88.63	88.99	89.21	91.54
Ti-O-Ti	*l*	°	99.08	99.65	99.47	99.22	98.90	98.75	98.58	95.76
Ti-O-*A*	*m*	°	125.99	126.34	126.13	126.88	126.69	126.43	127.24	128.01
Ti-O-*A*	*n*	°	87.97	87.52	87.22	87.15	87.16	87.54	87.52	86.49
Ti-O-*A*	*o*	°	137.18	136.50	136.50	135.99	136.28	136.71	135.88	134.52

The data of Kidoh *et al.* (1984) were used for $MnTiO_3$.
The metal–metal distances: *a* across shared edge between adjacent metal sites; *b* across the vacant octahedral position.
The oxygen–oxygen distances: *c* *A*–Ti shared face; *d* *A* site, face opposite the shared face; *e* *A* site, shared edge; *f* *A* site, unshared edge; *g* Ti site, face opposite the shared face; *h* Ti site, shared edge; *i* Ti site, unshared edge.
Framework angles: *j*, *m*, and *o* at the shared vertex; *k* and *l* at the shared edge; *n* shared face.